



Science Arts & Métiers (SAM)

is an open access repository that collects the work of Arts et Métiers Institute of Technology researchers and makes it freely available over the web where possible.

This is an author-deposited version published in: <https://sam.ensam.eu>
Handle ID: <http://hdl.handle.net/10985/21736>



This document is available under CC BY-NC license

To cite this version :


Mohammad AHMADIFAR, Mohammadali SHIRINBAYAN, Khaled BENFRIHA, Abbas TCHARKHTCHI, Joseph FITOUSSI - Mechanical behavior of polymer-based composites using fused filament fabrication under monotonic and fatigue loadings - Polymers and Polymer Composites - Vol. 30, p.096739112210824 - 2022

Any correspondence concerning this service should be sent to the repository

Administrator : scienceouverte@ensam.eu



Mechanical behavior of polymer-based composites using fused filament fabrication under monotonic and fatigue loadings

Polymers and Polymer Composites
Volume 30: 1–11
© The Author(s) 2022
Article reuse guidelines:
sagepub.com/journals-permissions
DOI: 10.1177/09673911221082480
journals.sagepub.com/home/ppc


Mohammad Ahmadifar^{1,2}, Khaled Benfriha², Mohammadali Shirinbayan¹ , Joseph Fitoussi¹ and Abbas Tcharkhtchi¹

Abstract

The use of additive manufacturing has been widely developed in the industry due to its ability to make complex shapes. The use of reinforcing fibers has provided a wider design capability in this field. Due to the effect of the number of fibers reinforced used on the mechanical properties, the study of the obtained mechanical properties is of great importance. This paper presents the experimental findings of tensile loading and three points bending fatigue tests performed on polymer-based composites (Onyx (which is CF-PA6) and reinforced Onyx with continuous glass fiber (CF-PA6 + GF) using Fused Filament Fabrication. Tensile properties of various types of printing conditions (Solid, Triangular, Rectangular, and Hexagonal fill patterns) have been compared. The coupled frequency amplitude affects the nature of the overall fatigue response which can be controlled by the damage mechanisms accumulation and/or by the self-heating. For fatigue loading, self-heating has been observed and yielded a temperature rise to about 60°C which is more than the glass transition temperature of the polymer. Multi-scale damage analysis of the sample in fatigue showed that the first observed damage phenomenon corresponds to the debonding of the filaments which leads to the propagation of transverse cracks.

Keywords

fatigue analysis, damage, fused filament fabrication, viscoelastic properties

Received 13 April 2021; accepted 21 January 2022

Introduction

Additive manufacturing (AM), or rapid prototyping (RP), or solid-freeform (SFF), also known as the 3D printing process^{1–5} is a new generation of the manufacturing method of the parts. Different additive manufacturing methods are oriented to fabricate the different functional parts in the last 20 years. In fact, AM methods have been used in different industries such as the aerospace industry,^{6,7} medical applications,^{4,8–12} automobile industries,^{6,7} construction,^{13–16} and so forth. Additive manufacturing (AM) is a novel technology that enables the rapid fabrication of physical models directly from 3D computer-aided design (CAD) data with no conventional tooling or programming requirement.

The most popular SFF technologies to date are Stereo-lithography (SL), Laminated object manufacturing (LOM), Fused Filament Fabrication (FFF), Selective laser sintering (SLS), and Multi-jet modeling (MJM).^{17,18} Among all the stated AM fabricating methods above, fused filament fabrication (FFF) (which is known as Fused Deposition Modeling (FDM)) and Selective Laser Sintering (SLS) have been the most used rapid prototyping (RP) methods for the fabrication of polymer composite parts. As for the comparison between FFF and SLA methods, FFF parts have lower mechanical properties.¹⁹ But FFF has some advantages such as less expensive materials and machines, which result in a cost-effective process,²⁰ and minimum waste of the used materials.

¹Arts et Metiers Institute of Technology, CNAM, PIMM, HESAM University, Paris, France

²Arts et Metiers Institute of Technology, CNAM, LCPI, HESAM University, Paris, France

Corresponding authors:

Mohammad Ahmadifar, Arts et Metiers Institute of Technology, 151 Boulevard de l'Hôpital, Paris 75013, France.

Email: mohammad.ahmadifar@ensam.eu

Mohammadali Shirinbayan, Arts et Metiers Institute of Technology, 151 Boulevard de l'Hôpital, Paris 75013, France.

Email: mohammadali.shirinbayan@ensam.eu



Generally, fused filament fabrication (FDM) is one of the most common and widely used AM technologies. As for a brief introduction, the raw material, which is in rolled filament form (feedstock), is fed into a machine via a pinch roller mechanism. The feedstock is melted in a heated liquefier section. Also, the un-melted part of the feedstock, which is the solid portion of the filament acting as a piston to push the melt through a print nozzle, then is deposited on the platform (bed). The extruded material (polymer (s) or polymer composite) solidifies and adheres, to the previous printed and solidified layers rapidly, to fabricate the complex desired parts.²¹

Mostly, the used feedstocks for FFF are thermoplastic with low levels of crystallinity or amorphous according to have as little shrinkage as possible in the final fabricated parts. Using the FFF process for the manufacturing of composite parts is increased in recent years. It is observed that the use of reinforcement has improved the benefits of shrinkage and strength, both.²² Also, one of the stated aims of the reinforcements usage in FFF is to overcome the non-printability of some raw materials, related to their high coefficient of linear thermal expansion.^{22,23}

Lectcher and Waytashek,²⁴ have studied the fatigue behavior of the 3D-printed PLA specimens. They used “Makerbot Replicator 2x” 3D-printer and studied the effect of the raster angle by choosing the, 0°, 45°, and 90° raster angles. Their fatigue tests were applied in the range of 2–20 Hz as frequencies under the fully reversed sinusoidal axial force. According to their result, it was found out that manufacturing direction has effects on the fused deposition modeling processed PLA samples. Similarly, Afrose et al.²⁵ have studied the fatigue behavior of the 3D-printed PLA specimens by the “Cube-2” 3D printer. They had experimental studied on the effect of the build orientation on the fatigue behavior of fused deposition modeling processed PLA dog-bone flat specimens. The fatigue test was applied under the 1 Hz, as frequency. Their results showed that related ultimate tensile stress of printed samples in X-direction (0°) was the highest which was 38.7 MPa. The related ultimate tensile strength values of the printed samples in Y-direction (90°) and 45°-direction were 31.1 and 33.6 MPa, respectively. But 45°-direction printed samples had the highest fatigue life in comparison with printed ones on the X- and Y-directions. Ezeh and Susmel²⁶ reported the fatigue behaviors of the 3D-printed PLA samples by considering mean stress effects, and also a unifying design curve was proposed. Ziemian et al.²⁷ applied tensile-fatigue tests on the manufactured ABS samples by FDM. According to the results, the printed samples with raster orientation at +45/−45° had higher fatigue life and a higher storage modulus, than the 0°, 45°, and 90° printed ones. Imeri et al.²⁸ studied on fatigue behavior of fiber-reinforced additive manufacturing specimens, printed by “Markforged Mark Two 3D printer.” They analyzed the data collected with analysis of variance (ANOVA) according to investigate the importance of some printing parameters. According to the results, a correlation between the type of reinforcements and the printing pattern of reinforcements was found out. As for the effect of the used reinforcement, carbon fiber showed better fatigue life. Also, as the effect of the printing pattern of reinforcements, the fatigue life performance was improved by the use of more rings of reinforcement. But, in the case of concentric infill, the fatigue performance decreased by an increase in the number of rings. Alberto D. Pertuz et al.²⁹ studied the effect of filling percentage, filling pattern of the nylon matrix, fiber materials (glass fiber, Kevlar, and carbon fibers), fiber orientation, and the number of concentric rings used in the printing configuration, in the printed samples by MarkForged Mark Two printer. The printed nylon matrix samples in triangular filling pattern and matrix density of 20%, by use of the carbon fiber reinforcement at 0-degrees, had better fatigue performance. Lee et al.³⁰ studied the printed ABS and ABS-plus samples by FDM. They have studied the effect of the printing orientations on the fatigue performance of 3D-printed samples.

One may therefore conclude that the mechanical properties of 3d-printed pieces are limited. In this work, the mechanical properties have been improved by reinforcing with the fibers such as s, carbon fibers, etc. The used material as raw material was Onyx, which was CF-PA6. Onyx is introduced as one of the newest matrix materials for fabricating composite parts with Markforged 3D printers. The Onyx (or CF-PA6), which has been introduced as a matrix for fabricating the polymer composite parts, is composite by itself. First, after some physical-chemical characterizations, various types of printing conditions (solid, triangular, rectangular, and hexagonal fill patterns) have been performed and the comparison between them in term of tensile properties have been done. Then, the continuous glass fiber was used for manufacturing the reinforced CF-PA6 with continuous glass fiber (FDM of composite) and some analyses were presented.

The structure of this article is as follows: the section of material description and methods is dedicated to a description of the main physico-chemical characteristics and the modeling of the viscoelastic behavior of Onyx using the DMA test. The developed experimental procedure for fatigue testing at several amplitudes has been performed. In the experimental results and discussion section, the obtained experimental results from applying the quasi-static and fatigue loadings and multi-scale damage analysis are presented and discussed.

Material description, 3D printer device, and characterization methods

Raw material

Carbon fiber-reinforced PA6 composites (CF-PA6). The used raw material was a filament of reinforced PA6 by about 6.5Wt% chopped carbon fiber (CF-PA6), with the commercial name of Onyx. Onyx (CF-PA6), which has also been introduced as a matrix for fabricating the polymer composite parts, also is composite by itself, too. It is a sort of combination and fusion of engineering plastic as its matrix and chopped carbon fibers as its reinforcements with the mass content of 6.51% in 93.49% of the matrix. It is a specially tuned PA6 copolymer (polyamide) filament with a chopped carbon fiber blend, adding great strength and stiffness unique to FFF printing. The infill patterns of the manufactured short carbon fiber-reinforced composites

specimens were triangular, rectangular, hexagonal, and solid infill. Already, Ahmadifar et al.,³¹ have studied the effect of some main process parameters on the thermal and mechanical behavior of Onyx.

Reinforced (CF-PA6) with continuous glass fiber. By Mark Two it is possible to print the continuous reinforcements in concentric or/and isotropic patterns. By choosing the Isotropic infill pattern, the designer will be capable to consider the specific printing direction(s) for the continuous reinforcement. The isotropic infill pattern was chosen as the continuous reinforcement printing pattern. The printing directions of the reinforcement layers -0° and 45° (Figure 1) were considered to decrease the anisotropic behavior of additive manufactured specimens. The glass fiber was used as the continuous reinforcement material. The specimens were manufactured in forty layers (the number of the matrix and reinforcement layers, both). Four layers were considered as the number of reinforcement layers. The glass fibers were deposited as sixth, seventh, thirty-fourth, and thirty-fifth layers.

3D printer device

One of Markforged's desktop printers is Mark Two Printer. In this research, the used 3D Printer device was Mark two printer (Figure 2). This printer manufactures the parts from Nylon (PA6) or Onyx (CF-PA6) materials which have been developed by Markforged. By the way, it is possible to use continuous reinforcement fibers of carbon or, glass, or Kevlar. Some stated technical specifications for Mark Two printer are listed in Table 1.²¹ This printer has two extruders, one of them is allocated to deposit the matrix material and another one is allocated to the reinforcement materials. So, the temperature of each nozzle will not be the same.

As was stated, Mark Two can fabricate the different structures at different percentages. According to the related printer software, it is possible to choose three dominant types of structure, which are rectangular, triangular, and hexagonal. Also, during our study, we sort of consider the solid fill printing condition, as another structure or infill pattern, as its different structure from the other ones. In fact, in the solid fill pattern, the raster orientations of the layers were $+45^\circ$, -45° , $+45^\circ$, -45° , ... The used temperature for the printing process of CF-PA6 (Matrix material) and Glass fiber (reinforcement material), were about 276°C and 253°C , respectively.

Methods of characterization and experimental procedure

Microscopic observation. The ZEISS optical microscope was used to observe the used CF-PA6 filament and orientation of chopped carbon in the filament. Microscopic observations and image analysis, using scanning electronic microscope (HITACHI 4800 SEM), have been done to qualitatively examine the composite microstructure, especially damage analysis.

Differential scanning calorimetric (DSC). DSC measures specific heat capacity by heating a sample and measuring the temperature difference between the sample and a reference. This method is used for measuring the melting points, glass transition, crystallization temperature, and the heat capacity of the used CF-PA6 filament. the measurement was carried out using the DSC Q10.

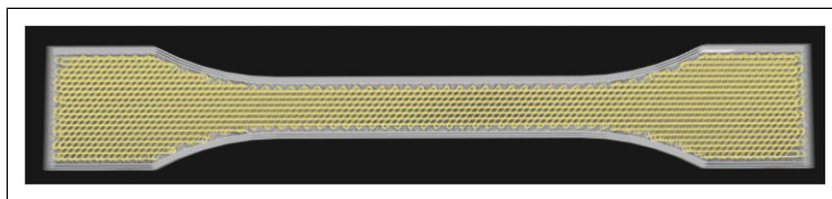


Figure 1. Orientation of the deposited glass fiber.

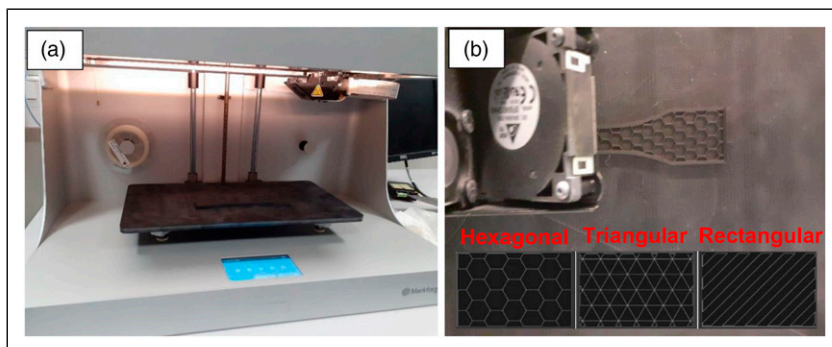


Figure 2. Mark Two printer (a) and printer during the print of the required specimens (b).

DMTA measurement. Thermo-mechanical analysis (DMTA) flexural tests have been attained to measure the major transitions temperatures on the printed sample made of CF-PA6, using the DMA Q800 instrument from TA Company. The flexural test has been realized at the following condition: temperature range varying from 30 to 80°C, temperature rate of 2°C/min, and the frequencies of 1, 2, 5, 10, and 30 Hz.

Quasi-static tensile test. The used sample was according to the standard ISO 527-1. Quasi-static tensile experiments have been achieved with the INSTRON 5966 machine, loading cell of 10 kN, and the displacement rate is 5 mm/min. In order to the reproducibility of the results, at least four samples were carried out in the Tensile Test study.

Fatigue test. Three points bending fatigue tests have been performed at different applied maximum strains (ϵ_{\max}). The minimum applied strain (ϵ_{\min}) was chosen to be equal to 10% of the maximum applied strain. The chosen strain-ratio was thus ($R_{\sigma} = 0.1$), and the mean strain-level was equal to $0.55 \epsilon_{\max}$.

During fatigue loading, the temperature rise, due to the composite self-heating, has been measured on the surface of the specimen using an infrared camera (Raynger- MX4). An Optris PI450 infrared camera was used (Figure 3).

Multi-scale damage analysis in fatigue. The macroscopic damage evolutions have been estimated through the measurement of Young's modulus evolutions. Microscopic damage observations were performed by subjecting CF-PA6 specimens to a fatigue loading under specific loading amplitude with a frequency of 10 Hz. The observation area corresponded to a polished thickness surface of the rectangular composite with a geometry of $120 \times 10 \times 4 \text{ mm}^3$.

Experimental results and discussion

Microstructure analysis

According to the observation of the carbon fibers (Microscopy Observation) under the optical microscopy, the size range of the disturbed chopped carbon fibers was about 10 to 312 micrometers, according to Figure 4(a). Note that the diameter of the used CF-PA6 filament was 1.75 mm. According to the optical observation of the used filament (Figure 4(b)), the chopped carbons of the CF-PA6 filament, were directional.

Moreover, the microstructure of CF-PA6 reinforced with glass fiber can be observed in Figure 4(c). The continuous glass fiber is marked at the top of Figure 4(c).

Thermo-mechanical properties

Thermal analysis. Table 2 shows the results of the DSC test with a heating rate of 10°C/min for the CF-PA6 filament. The glass transition temperature, the crystallization temperature, and the melting temperature of this test, respectively, are reported in Table 2.

Thermo-mechanical properties

Glass transition temperature. Main transition temperatures due to molecular mobility as a function of the temperature have been measured using the DMTA test. This test can be useful to analyze the induced self-heating phenomenon and to relate it to the

Table 1. Technical specifications for mark two printer.

Build volume	320 mm x 132 mm x 154 mm
Plastics available	Onyx, Nylon white
Fibers available	Carbon fiber, glass fiber, Kevlar, HSHT glass fiber (High-Strength High-Temperature Glass fiber)
Layer height	100 μm default
Infill	Closed-cell infill: multiple geometries available

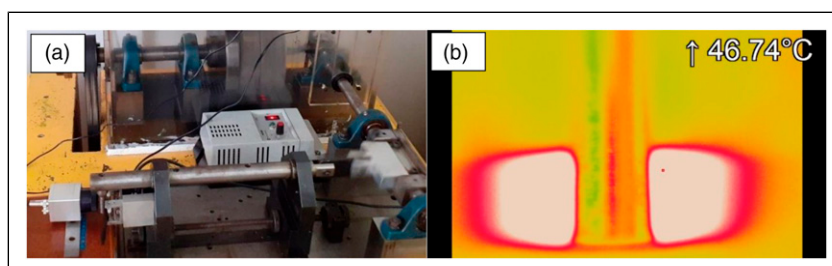


Figure 3. The sample under the three-point bending fatigue test (a) temperature measurement during the fatigue test by the infrared camera (b).

measured temperature rise during a fatigue test at different amplitudes. Figure 5 shows the evolution of the storage and loss moduli versus temperature on the CF-PA6 sample. As it can be noticed, CF-PA6 presented a glass transition of nearly 60°C.

The elastic or viscous response of CF-PA6 can be measured as a function of temperature using DMTA; it is possible to understand the true internal damping of the system. One can suppose that CF-PA6 has rigid stability at ambient temperature while the storage modulus continuous to decrease slowly until 80°C due to the increase of macromolecular chain mobility.

Viscoelasticity modeling by Cole-Cole principle. Various approaches have been used to study the viscoelastic properties in the temperature range between the glassy and rubbery domain, and different models have been proposed to predict these properties. These models generally represent the curve of E'' (loss modulus) as a function of E' (storage modulus), and the curve is known as the Cole-Cole diagram. For the validation of the theoretical model, experimental data obtained by the dynamic mechanical, thermal analysis (DMTA) tests are required. After DMTA tests, an asymmetric Cole-Cole diagram has been plotted (Figure 6). The behavior of polymers can be analyzed by the bi-parabolic model according to the Perez model, the equation is as follow

$$E^* = E_0 + \frac{E_\infty - E_0}{1 + (i\omega\tau)^k + Q(i\omega\tau)^{k'}} = E' + iE'' \quad (1)$$

with

$$E' = E_0 + (E_\infty - E_0) \frac{1 + \cos\left(\frac{k\pi}{2}\right)(\omega\tau)^{-k} + Q \cos\left(\frac{k'\pi}{2}\right)(\omega\tau)^{-k'}}{D} \quad (2)$$

$$E'' = (E_\infty - E_0) \frac{\sin\left(\frac{k\pi}{2}\right)(\omega\tau)^{-k} + Q \sin\left(\frac{k'\pi}{2}\right)(\omega\tau)^{-k'}}{D} \quad (3)$$

and

$$D = \left[1 + \cos\left(\frac{k\pi}{2}\right)(\omega\tau)^{-k} + Q \cos\left(\frac{k'\pi}{2}\right)(\omega\tau)^{-k'} \right]^2 + \left[\sin\left(\frac{k\pi}{2}\right)(\omega\tau)^{-k} + Q \sin\left(\frac{k'\pi}{2}\right)(\omega\tau)^{-k'} \right]^2 \quad (4)$$

where k and k' and Q are the constants of this model. $\omega = 2\pi f$ is the angular frequency (f = frequency) Furthermore, E^* is the complex shear modulus: E_∞ and E_0 are the value of modulus at the, respectively, glassy and rubbery states. k and k' depend on

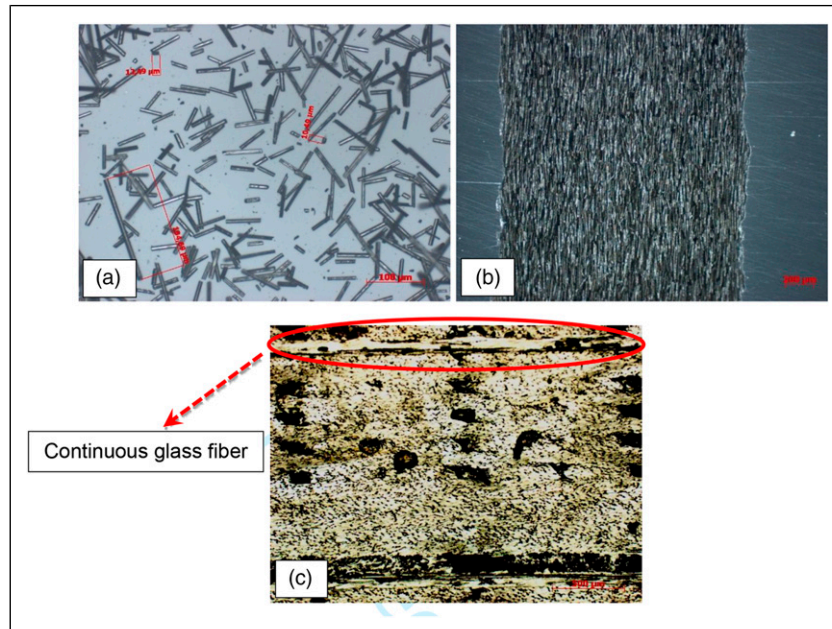


Figure 4. Microscopy observation of the chopped carbon fibers in the used filament (a), CF-PA6 filament (b), and CF-PA6 reinforced with continuous glass fiber (c).

Table 2. Thermal properties of the used CF-PA6 filament.

T_g (°C)	T_c (°C)	T_m (°C)
61	162	198

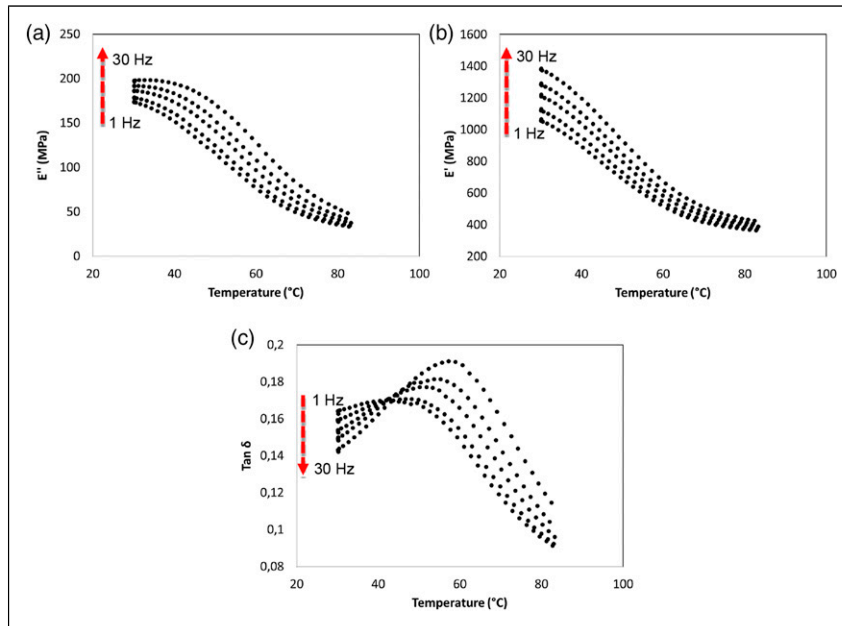


Figure 5. DMTA test result: Evolution of the storage, loss moduli, and loss factor versus temperature.

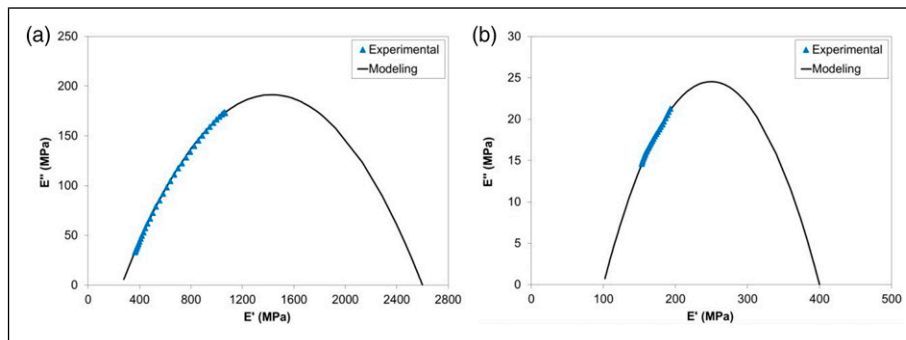


Figure 6. Cole-Cole plot of (a) CF-PA6 + GF and (b) CF-PA6.

the slope of the tangents at the beginning and the end of the Cole-Cole diagram (dE''/dE'), Q is a constant related to the maximum value of E'' . τ is the average relaxation time.

The values of the model's parameters are shown in Table 3. The theoretical curve fits perfectly with the experimental results, signifying that the bi-parabolic model can accurately predict the viscoelastic behavior of CF6.51-PA6.

Quasi-static tensile behavior

Effect of fill patterns. As it was stated, the three main infill patterns which were triangular, rectangular, and hexagonal were considered to print the tensile specimens, by Mark Two printer. So, the tensile samples were printed by use of the CF-PA6 filament under these stated main infill patterns. Their tensile strength was compared with each other and also with the solid infill pattern (whose infill percentage was 100%). So, the tensile strength was considered as the criterion to make the comparison. The Tensile test results of the different infill pattern samples, which were made of CF-PA6 are listed in Figure 7 and Table 4.

According to the tensile test results of the printed samples by the use of CF-PA6, the tensile strength of triangular, rectangular, hexagonal, and solid infill were 18.79 ± 1.19 , 19.84 ± 1.66 , 19.99 ± 2.32 , and 30.31 ± 5.5 (MPa), respectively. So, as it is clear, the tensile strength of the triangular specimens is the lowest in comparison with the other infill patterns. Then the rectangular infill patterns are more than triangular, but less than hexagonal. The most tensile strength is related to the solid infill samples. As it was extracted from the results, by changing the infill pattern of the printed CF-PA6 samples from triangular to rectangular and hexagonal, the tensile strength has been improved 5.9% and 6.4%, respectively. But by changing the infill pattern of the printing process of the samples which were made of CF-PA6, from the triangular to solid infill, the tensile strength improved almost 61.3% (Figure 7).

Effect of the continuous reinforcement on different infill patterns. The Tensile samples were printed by use of the CF-PA6 filament and continuous glass fiber, under the main stated infill patterns. Again, their tensile strength was compared with each other and

also with the solid infill pattern (whose infill percentage was 100%). So, the tensile strength was considered as the criterion to make the comparison. The tensile test results of the different infill pattern samples, which were made of CF-PA6 reinforced with continuous glass fiber, are in Figure 8. According to the tensile test results of the printed samples by use of CF-PA6 reinforced continuous glass fiber, the tensile strength of hexagonal, rectangular, triangular and solid infill were 60.04 ± 4.16 , 66.7 ± 2.63 , 69.6 ± 3.05 , and 78.35 ± 0.87 (MPa), respectively. So, as is clear, the tensile strength of the hexagonal specimens are the lowest in comparison with other infill patterns. Then the rectangular infill patterns are more than hexagonal, but less than triangular. The most tensile strength is related to the solid infill samples. As it was extracted from the results, by changing the infill pattern of the printed CF-PA6 reinforced with continuous glass fiber samples from hexagonal to rectangular and triangular, the tensile strength has been improved 11.1% and 15.92%, respectively. But, by changing the infill pattern of the printing of the samples which were made of CF-PA6 and continuous glass fiber, from the hexagonal to solid infill, the tensile strength improved almost 30.5% (Figure 8). In fact, by use of continuous glass fiber, the strength of the solid infill samples, increased about 158.5%, respectively.

Fatigue behavior analysis

Effect of using the continuous reinforcement. Figure 9 shows the Wöhler curves obtained in three points bending fatigue tests at a frequency of 10 Hz for CF-PA6 (Onyx) and CF-PA6 reinforced with continuous glass fiber (Onyx+GF) samples.

The curves evidence the effect of the fiber reinforcement. One can note that in the case of the printed specimens with CF-PA6, for applied strain equal to 4.5%, the fatigue life is about 200,000 cycles whereas the fatigue life is about 2000 cycles for CF-PA6 reinforced with continuous glass fiber.

It can be established that for CF6-PA6 composite, the fatigue design can be efficiently optimized through glass fiber reinforcement. Regarding CF-PA6 reinforced with continuous glass fiber samples at 10 Hz, it can be noted that the Wöhler curve shows a linear form. However, for the CF-PA6 sample a bi-linear form can be observed.

Wöhler curves obtained from fatigue tests for CF-PA6 and CF-PA6 reinforced with continuous are shown in Figure 9. One can indicate that there is a small difference between the curves at high amplitude while at low strain amplitude, the Wöhler curve is shifted.

Relative Young's modulus evolution and self-heating phenomenon. Figure 10 shows the evolution of the relative stress during fatigue tests for CF-PA6 and CF-PA6 reinforced with continuous glass fiber samples at the frequency of 10 Hz. All samples exhibit a fatigue behavior mostly governed by the Mechanical Fatigue (MF) nature due to damage phenomenon, whereas for high amplitude, the Induced Thermal Fatigue (ITF) is the predominant nature of the fatigue behavior at low cycles for CF-PA6 and CF-PA6 reinforced with continuous glass fiber samples. The detailed analysis of MF and ITF has been presented in previous work.³²

From these curves, one can observe that for high loading amplitudes, the dynamic modulus decreases rapidly in a linear regime of the logarithmic curve until the failure of the specimen. For low applied amplitudes, the dynamic modulus exhibit three decreasing regimes a rapid one during the initial cycles (I), followed by a gradual one (II), and finally a drastic decrease (III) just before the fracture. One can note that the significant damage kinetic in the case of CF-PA6 reinforced with continuous glass fiber (Onyx+GF).

Varying the loading conditions in terms of amplitude, the fatigue behavior of CF-PA6 and CF-PA6 reinforced with continuous glass fiber induces self-heating. This phenomenon influences the viscous behavior of the polymer as a function of

Table 3. Perez model parameters for CF-PA6 and CF-PA6 + GF.

Material	Frequencies (Hz)	E_0 (MPa)	E_∞ (MPa)	k	k'	Q	τ (s)
CF-PA6	1	100	400	0.2	0.22	0.5	0.5
CF-PA6 + GF	1	260	2600	0.2	0.22	0.5	0.5

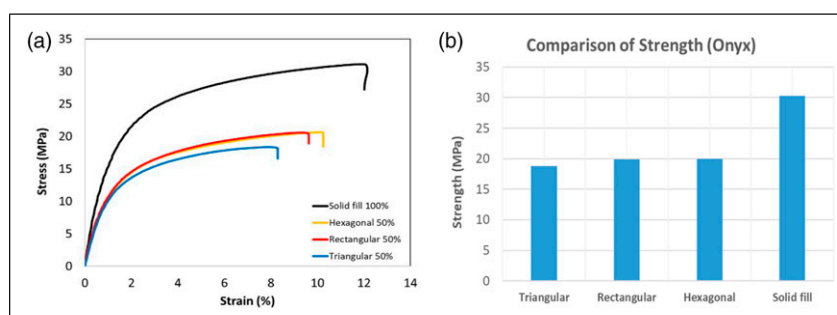
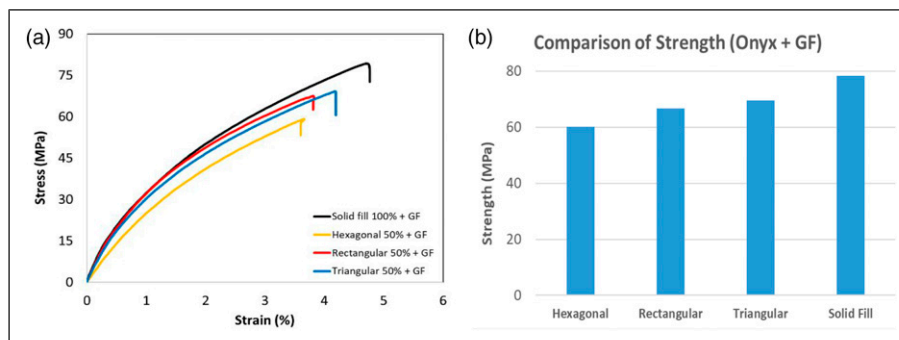


Figure 7. Quasi-static tensile curves (a) and strength evolution (b).

Table 4. Tensile test results of the printed samples under the different infill patterns, made of CF-PA6.

Triangular infill pattern samples, made of CF-PA6					
SAMPLE	E (MPa)	σ_{\max} (MPa)	ϵ_{\max}	σ_y	ϵ_y
1	15	20.25	8.3	5.2	0.31
2	16	19.10	8.2	4.8	0.33
3	15	18.4	8	4.1	0.3
4	15	17.41	7	5.9	0.4
AVERAGE	15.25	18.79	7.87	5	0.34
STDEV	0.5	1.19	0.59	0.75	0.04
Rectangular infill pattern samples, made of CF-PA6					
Sample	E (MPa)	σ_{\max} (MPa)	ϵ_{\max}	σ_y	ϵ_y
1	13	18.8	9.7	4.4	0.36
2	18	21.8	8.9	5.9	0.33
3	17	18.17	10.53	3	0.2
4	17	20.6	9.30	4.7	0.3
Average	16.25	19.84	9.61	4.5	0.3
STDEV	2.22	1.66	0.7	1.19	0.07
Hexagonal infill pattern samples, made of CF-PA6					
Sample	E (MPa)	σ_{\max} (MPa)	ϵ_{\max}	σ_y	ϵ_y
1	13	16.85	8.3	5.2	0.31
2	15	20.06	8.2	4.8	0.33
3	15	20.67	8	4.1	0.3
4	16	22.41	7	5.9	0.4
Average	14.75	19.99	7.88	5	0.34
STDEV	1.26	2.32	0.6	0.75	0.05
Solid infill samples, made of CF-PA6					
Sample	E (MPa)	σ_{\max} (MPa)	ϵ_{\max}	σ_y	ϵ_y
1	23	31.15	11.94	7.7	0.36
2	18	24.1	10.8	5.41	0.32
3	24	37.3	11.8	10.76	0.42
4	21	28.7	12.8	5.15	0.26
Average	21.5	30.31	11.84	7.26	0.34
STDEV	2.65	5.5	0.82	2.6	0.07

**Figure 8.** (a) Quasi-static tensile curves and (b) Strength evolution.

the temperature rise level concerning material transition temperatures. In the case of CF-PA6 samples, for the test performed at 10 Hz, the temperature increases up to 60°C (Figure 11). This temperature corresponds to the glass transition zone. At this stage, the polymer stiffness slightly decreases as shown in Figure 5. Therefore, the polymer matrix is subjected to extraordinary thermally activated modifications of its physical state.

Hence, at the microscopic scale, the fatigue behavior and failure of printed CF-PA6 samples are not only due to the devolvement of diffuse damage but also to the evolution of the viscous behavior of the polymer and the inherent brittle–ductile transition. The evolution of temperature is one of the critical parameters in fatigue. Maximum induced temperature can be a

factor in predicting the fatigue behavior of CF-PA6 and reinforced CF-PA6 with continuous glass fiber and the state of polymer in terms of ductility. Figure 11, illustrates the maximum induced temperature just before failure. Figure 11, presents the influence of reinforcement on the maximum induced temperature.

One can observe the same slope of the curve for two cases. As was mentioned, there are two types of fatigue: MF and ITF. By considering the glass transition temperature of about 61°C, the critical fatigue tests with induced thermal fatigue can be separated. Moreover, one can note that the induced temperature for all applied strains is higher in the case of CF-PA6 (without continuous reinforcement).

Fatigue fracture surface. For emphasizing the effect of loading amplitude at a microscopic scale fracture, surface observations have been performed. Figure 12, compares the fracture surfaces of the printed CF-PA6 and CF-PA6 reinforced with continuous glass fiber samples. SEM analysis highlights these conclusions:

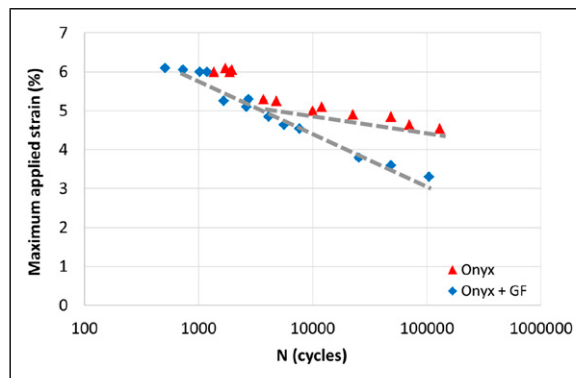


Figure 9. Wöhler curves for CF-PA6 (Onyx) and CF-PA6 reinforced with continuous glass fiber (Onyx+GF) samples at 10 Hz.

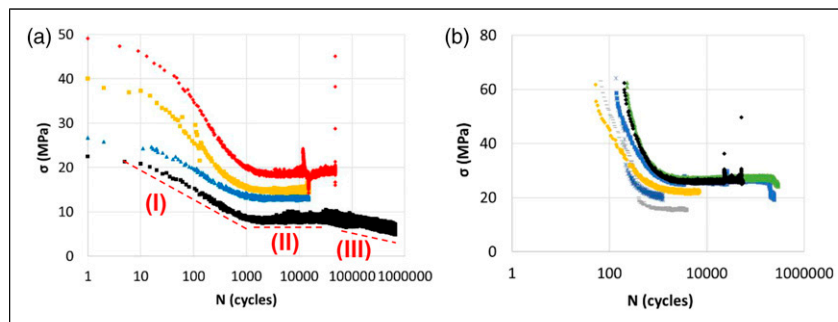


Figure 10. Evolutions of the relative stress (~Young’s modulus) during fatigue tests for (a) CF-PA6 (Onyx) and (b) CF-PA6 reinforced with continuous glass fiber (Onyx+GF) samples.

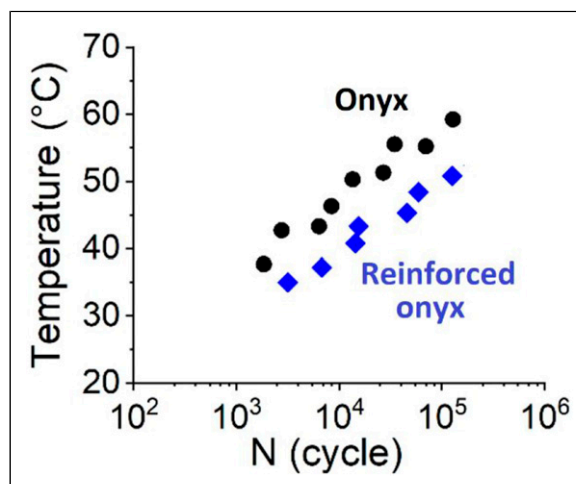


Figure 11. Maximum induced temperature evolution versus the number of cycles.

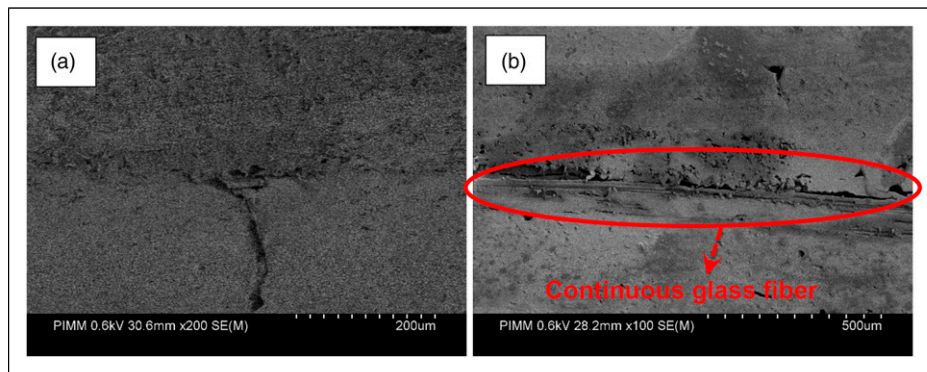


Figure 12. Fracture surface observations for CF-PA6 (a), and CF-PA6 reinforced with continuous glass fiber (b) samples.

- For the printed CF-PA6 samples, the first observed damage phenomenon corresponds to the debonding of the filament. This leads to the propagation of interphase cracking. For a higher value of cycles, this damage mechanism is spreading through the whole observation zone (Figure 12(a)).
- The fracture surface observation in the case of CF-PA6 reinforced with continuous glass fiber samples, showed that the bundles of fibers are pulled out from CF-PA6 simultaneously with breakage of the more surrounding matrix (Figure 12(b)).

Conclusion

In the present work, polymer-based composites using Fused Filament Fabrication (FFF) were prepared and submitted to tension and three points bending fatigue loadings. The main conclusion for this paper is as follows: first, the homogeneous distribution of carbon fiber in used Onyx (CF-PA6) filament was observed through the microscopy observation. The printed CF-PA6 samples in solid infill pattern, have excellent stiffness and mechanical properties under tension. In fatigue, the effect of reinforcement has been analyzed. The results showed that the induced temperature is increased and as a result, the fatigue life is decreased for and reinforced CF6.51-PA6. This phenomenon, which is known as self-heating, can evaluate the viscous behavior of the polymer especially in the glass transition zone (about 60°C). Therefore, it is necessary to study the viscoelastic behavior of CF-PA6. Perez model could predict the viscoelastic behavior of CF-PA6 and CF-PA6 reinforced with continuous glass fiber. Finally, damage mechanisms development in fatigue has been investigated at the microscopic scale. For CF-PA6 and reinforced CF-PA6 with continuous glass fiber, the first observed damage phenomenon corresponds to the debonding of the filaments which leads to the propagation of cracking.

Declaration of conflicting interests

The author(s) declared no potential conflicts of interest with respect to the research, authorship, and/or publication of this article.

Funding

The author(s) received no financial support for the research, authorship, and/or publication of this article.

ORCID iD

Mohammadali Shirinbayan  <https://orcid.org/0000-0002-2757-8529>

References

1. Ahmadifar M, Benfriha K, Shirinbayan M, et al. Additive manufacturing of polymer-based composites using fused filament fabrication (FFF): a review. *Appl Compos Mater* 2021; 28: 1335–1380.
2. Wang J, Xie H, Weng Z, et al. A novel approach to improve mechanical properties of parts fabricated by fused deposition modeling. *Mater Des* 2016; 105: 152–159.
3. Thomas DB, Hiscox JD, Dixon BJ, et al. 3D scanning and printing skeletal tissues for anatomy education. *J Anat* 2016; 229(3): 473–481.
4. Wu CS, Liao HT and Cai YX. Characterisation, biodegradability and application of palm fibre-reinforced polyhydroxyalkanoate composites. *Polym Degrad Stab* 2017; 140: 55–63.
5. Gardner JM, Hunt KA, Ebel AB, et al. Machines as craftsmen: localized parameter setting optimization for fused filament fabrication 3D printing. *Adv Mater Technol* 2019; 4(3): 1800653.
6. Ahn SH, Lee KT, Kim HJ, et al. Smart soft composite: an integrated 3D soft morphing structure using bend-twist coupling of anisotropic materials. *Int J Precis Eng Manuf* 2012; 13(4): 631–634.

7. Ahmed NA and Page JR. Manufacture of an unmanned aerial vehicle (UAV) for advanced project design using 3D printing technology. *Appl Mech Mater* 2013; 397: 970–980.
8. Murphy SV and Atala A. 3D bioprinting of tissues and organs. *Nat Biotechnol* 2014; 32(8): 773–785.
9. Seliktar D, Dikovskiy D and Napedensky E. Bioprinting and tissue engineering: recent advances and future perspectives. *Israel J Chem* 2013; 53(9–10): 795–804.
10. Xu T, Zhao W, Zhu JM, et al. Complex heterogeneous tissue constructs containing multiple cell types prepared by inkjet printing technology. *Biomaterials* 2013; 34(1): 130–139.
11. Paulsen SJ and Miller JS. Tissue vascularization through 3D printing: will technology bring us flow? *Dev Dyn* 2015; 244(5): 629–640.
12. Stansbury JW and Idacavage MJ. 3D printing with polymers: challenges among expanding options and opportunities. *Dent Mater* 2016; 32(1): 54–64.
13. Bos F, Wolfs R, Ahmed Z, et al. Additive manufacturing of concrete in construction: potentials and challenges of 3D concrete printing. *Virtual Phys Prototyping* 2016; 11(3): 209–225.
14. Wu P, Wang J and Wang X. A critical review of the use of 3-D printing in the construction industry. *Autom Constr* 2016; 68: 21–31.
15. Hager I, Golonka A and Putanowicz R. 3D printing of buildings and building components as the future of sustainable construction? *Proced Eng* 2016; 151: 292–299.
16. Perkins I and Skitmore M. Three-dimensional printing in the construction industry: A review. *Int J Constr Manage* 2015; 15(1): 1–9.
17. Górski FI, Kuczko WI and Wichniarek RA. Impact strength of ABS parts manufactured using Fused Deposition Modeling technology. *Arch Mech Technol Autom* 2014; 34(1): 3–12.
18. Baich L, Manogharan G and Marie H. Study of infill print design on production cost-time of 3D printed ABS parts. *Int J Rapid Manuf* 2015; 5(3–4): 308–319.
19. Naranjo-Lozada J, Ahuett-Garza H, Orta-Castañón P, et al. produced by additive manufacturing. *Addit Manuf* 2019; 26: 227–241.
20. Wong KV and Hernandez A. A review of additive manufacturing. *Int Scholarly Res Not* 2012; 2012: 208760.
21. Tian X, Liu T, Yang C, et al. Interface and performance of 3D printed continuous carbon fiber reinforced PLA composites. *Compos Part A Appl Sci Manuf* 2016; 88: 198–205.
22. Stoof D and Pickering K. Sustainable composite fused deposition modelling filament using recycled pre-consumer polypropylene. *Compos Part B Eng* 2018; 135: 110–118.
23. Carneiro OS, Silva AF and Gomes R. Fused deposition modeling with polypropylene. *Mater Des* 2015; 83: 768–776.
24. Letcher T and Waytashek M. Material property testing of 3D-printed specimen in PLA on an entry-level 3D printer. In: ASME International mechanical engineering congress and exposition 14–20 2014 November, Montreal, Quebec, Canada, (Vol. 46438, p. V02AT02A014). American Society of Mechanical Engineers.
25. Afrose MF, Masood SH, Iovenitti P, et al. Effects of part build orientations on fatigue behaviour of FDM-processed PLA material. *Prog Additive Manuf* 2016; 1(1): 21–28.
26. Ezeh OH and Susmel L. Fatigue strength of additively manufactured polylactide (PLA): effect of raster angle and non-zero mean stresses. *Int J Fatigue* 2019; 126: 319–326.
27. Ziemian S, Okwara M and Ziemian CW. Tensile and fatigue behavior of layered acrylonitrile butadiene styrene. *Rapid Prototyping J* 2015. DOI: [10.1108/RPJ-09-2013-0086](https://doi.org/10.1108/RPJ-09-2013-0086)
28. Imeri A, Fidan I, Allen M, et al. Fatigue analysis of the fiber reinforced additively manufactured objects. *Int J Adv Manuf Technol* 2018; 98(9): 2717–2724.
29. Mohammadizadeh M. *Mechanical and thermal analyses of automotive components manufactured with 3D printed continuous fiber reinforced thermoplastic polymers* [Doctoral dissertation, Tennessee Technological University].
30. Lee J and Huang A. Fatigue analysis of FDM materials. *Rapid Prototyping J* 2013; 19(4): 291–299. DOI: [10.1108/13552541311323290](https://doi.org/10.1108/13552541311323290)
31. Benfriha K, Ahmadifar M, Shirinbayan M, et al. Effect of process parameters on thermal and mechanical properties of polymer-based composites using fused filament fabrication. *Polym Compos* 2021; 42: 6025–6037.
32. Shirinbayan M, Fitoussi J, Meraghni F, et al. Coupled effect of loading frequency and amplitude on the fatigue behavior of advanced sheet molding compound (A-SMC). *J Reinf Plast Compos* 2017; 36(4): 271–282.